Soft Matter

PAPER

View Article Online
View Journal | View Issue

Cite this: *Soft Matter*, 2014, **10**, 5121

Equilibrium phases of one-patch colloids with short-range attractions

Zdeněk Preisler,†*[ab] Teun Vissers,†[b] Gianmarco Munaò,[c] Frank Smallenburg[b] and Francesco Sciortino[b]

Received 5th March 2014
Accepted 29th April 2014

DOI: 10.1039/c4sm00505h

www.rsc.org/softmatter

Inspired by experimental studies of short-ranged attractive patchy particles, we study with computer simulations the phase behavior and the crystalline structures of one-patch colloids with an interaction range equal to 5% of the particle diameter. In particular, we study the effects of the patch surface coverage fraction, defined as the ratio between the attractive and the total surface of a particle. Using free-energy calculations and thermodynamic integration schemes, we evaluate the equilibrium phase diagrams for particles with patch coverage fractions of 30%, 50% and 60%. For a 60% surface coverage fraction, we observe stable lamellar crystals consisting of stacked bilayers that directly coexist with a low density fluid. Inside the coexistence region, we observe the formation of lamellar structures also in direct NVT simulations, indicating that the barrier of formation is low and experimental realization is feasible. For sufficiently strong interactions, these structures spontaneously assemble from the fluid in simulations, suggesting that they might also easily form in experimental systems. In the Janus case, *i.e.* at 50% surface coverage fraction, no lamellar structures are formed, and the stable crystals are similar to those that have been found previously for a longer interaction range (*i.e.* 20% of the particle diameter). At 30% coverage fraction, we identify novel 'open' crystal structures with large unit cells of up to 14 particles that are stable in the strong interaction limit.

I. Introduction

Colloidal particles with strongly directional interactions play an important role in soft matter physics. One way to achieve these interactions is by creating attractive patches on the colloids' surface[1–3] Current experimental techniques allow for the production of patchy colloids with different sizes, shapes and chemical compositions.[4–12] Because such particles exhibit strongly directional interactions, they constitute a useful tool to investigate the effects of the anisotropy on the self-assembly processes. In parallel with these experimental developments, significant theoretical and numerical efforts have been made to predict the physical properties of these systems[13,14] for example guiding the identification of empty liquids[15] in clay suspensions.[16] Patchy particles can be used to study fluid–fluid and fluid–solid phase transitions,[15,17] and even to create fluids that remain stable down to zero temperature.[18] Additionally, the influence of patch number and size, as well patchy properties in a binary mixture,[19–21] have been studied extensively. Of special interest is the diamond colloidal crystal found in particles with four patches in a tetrahedral geometry, because of its interesting photonic properties.[22–26]

One of the simplest examples of patchy colloids is provided by particles with a single patch, such as Janus particles with one attractive hemisphere.[10,27–34] The phase behavior of one-patch particles, as well as their self-assembly properties in external fields[35,36] and on interfaces[37,38] have been previously studied, demonstrating a rich phase behavior and the spontaneous self-assembly of micelles, vesicles, lamellae and tubes, analogous to aggregates found in molecular systems.[39–42]

In this work we address the issue of the sensitivity of the phase behavior of one-patch particles to the patch coverage fraction by numerical evaluation of equilibrium phase diagrams for the one-patch Kern–Frenkel (KF) model.[43] This model is frequently adopted in the context of colloidal systems with strongly directional attractions to investigate the structure, thermodynamics and self-assembly properties.[26,39,44–46] In the KF model, two particles bind if their mutual distance is within the range of the attraction, modeled by a square-well interaction, and their patches are properly aligned with each other. To be close to the experimental conditions,[32,47,48] we focus on a short (5% of the particle diameter) square-well range. In order to document the effect of the patch size on the relative thermodynamic stability of each phase we perform a thorough study for three different values of the patch coverage fraction χ, see Fig. 1.

[a]*Debye Institute for Nanomaterials Science, Utrecht University, Princetonplein 5, 3584CC, Utrecht, The Netherlands. E-mail: Z.Preisler@uu.nl*

[b]*Dipartimento di fisica, Sapienza, Università di Roma, Piazzale Aldo Moro 2, 00185, Roma, Italy*

[c]*Dipartimento di Fisica e di Scienze della Terra, Universit degli Studi di Messina, Viale F. Stagno d'Alcontres 31, 98166, Messina, Italy*

† These authors contributed equally.

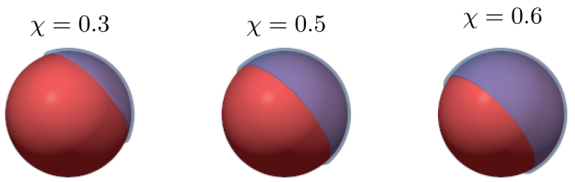

Fig. 1 One-patch particles interacting *via* a Kern–Frenkel potential for three different patch coverage fractions $\chi = 0.3$, $\chi = 0.5$ and $\chi = 0.6$. In the pictures the hard sphere particles are colored in red and the Kern–Frenkel potential bonding volume is depicted as transparent blue.

Following the strategy laid out in ref. 49, we employ a wide range of simulation techniques, including the floppy box method,[50] to find and characterize various crystalline structures. Subsequently, we employ free-energy calculations and thermodynamic integration methods to draw the phase diagrams and to calculate the thermodynamic stability of the crystal candidates and the fluid. In addition, we perform standard Monte Carlo calculations in the canonical ensemble (NVT) to characterize the spontaneous formation of the ordered phases. Finally, for $\chi = 0.5$, we evaluate the location of the gas–liquid critical point by performing successive umbrella sampling (SUS) simulations,[51] to assess the relative stability of the liquid phase with respect to crystallization.

II. The model

The advantage of using the Kern–Frenkel model is the possibility of a continuous interpolation from a pure square-well isotropic potential to the hard-sphere limit by tuning a simple parameter, the coverage fraction χ. This parameter is properly defined as the ratio between the attractive and the total surface. As a consequence, it assumes the values one and zero for the square-well and the hard-sphere potential, respectively. A schematic picture of the Kern–Frenkel is shown in Fig. 2.

Following Kern and Frenkel, the pair potential is written as a product of a square-well potential $u^{\mathrm{SW}}(r_{ij})$ and an angular dependence $\Omega(\mathbf{r}_{ij}, \hat{\mathbf{n}}_i, \hat{\mathbf{n}}_j)$, plus a hard sphere contribution $u^{\mathrm{HS}}(r_{ij})$. The potential u^{KF} is defined as

$$u^{\mathrm{KF}}(\mathbf{r}_{ij}, \hat{\mathbf{n}}_i, \hat{\mathbf{n}}_j) = u^{\mathrm{SW}}(r_{ij})\Omega(\mathbf{r}_{ij}, \hat{\mathbf{n}}_i, \hat{\mathbf{n}}_j) + u^{\mathrm{HS}}(r_{ij}), \quad (1)$$

The square-well potential $u^{\mathrm{SW}}(r_{ij})$ is

$$u^{\mathrm{SW}}(r_{ij}) = \begin{cases} -\varepsilon & \text{if } \sigma < r_{ij} \leq \sigma + \Delta \\ 0 & \text{otherwise,} \end{cases} \quad (2)$$

with σ the particle diameter, Δ the interaction range ($\Delta = 0.05\sigma$ in the present case) and ε the depth of the square well. The function $\Omega(\mathbf{r}_{ij}, \hat{\mathbf{n}}_i, \hat{\mathbf{n}}_j)$ depends on the orientations of two particles i and j

$$\Omega(\mathbf{r}_{ij}, \hat{\mathbf{n}}_i, \hat{\mathbf{n}}_j) = \begin{cases} 1 & \text{if} \begin{cases} \hat{\mathbf{r}}_{ij} \cdot \hat{\mathbf{n}}_i > \cos\theta & \text{and} \\ \hat{\mathbf{r}}_{ji} \cdot \hat{\mathbf{n}}_j > \cos\theta \end{cases} \\ 0 & \text{otherwise,} \end{cases} \quad (3)$$

where $\hat{\mathbf{n}}_i$ and $\hat{\mathbf{n}}_j$ denote the orientations of the patches of particles i and j respectively, and $\mathbf{r}_{ij}$ is the vector that joins the center of mass of the two particles. To ensure that the particles do not overlap, the KF potential includes a hard-sphere component $u^{\mathrm{HS}}(r_{ij})$ given by

$$u^{\mathrm{HS}}(r_{ij}) = \begin{cases} \infty & \text{if } r_{ij} \leq \sigma \\ 0 & \text{otherwise.} \end{cases} \quad (4)$$

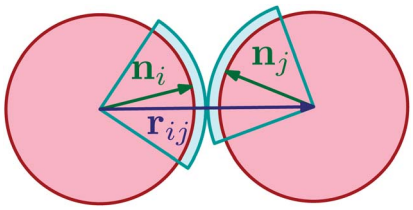

Fig. 2 Schematic representation of two patchy spheres interacting *via* a Kern–Frenkel potential (eqn (1)). The attractive bonding volumes are shown in blue. The vector $\mathbf{r}_{ij}$ points from particle i to particle j. The vectors $\hat{\mathbf{n}}_i$ and $\hat{\mathbf{n}}_j$ show the orientations of the particles i and j.

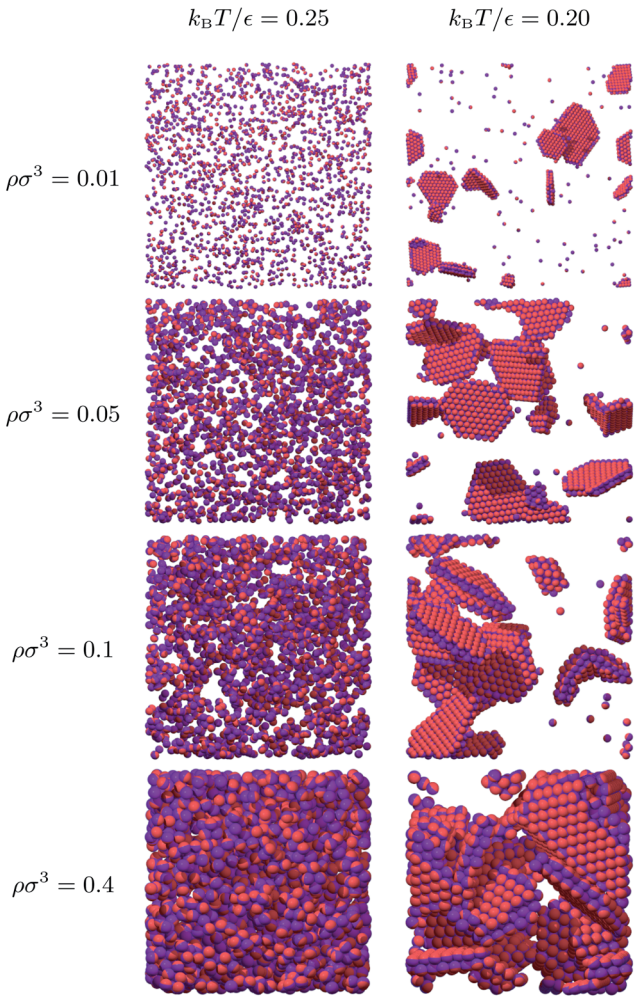

Fig. 3 Typical snapshots from constant NVT simulations of particle configurations at $\chi = 0.6$, $k_{\mathrm{B}}T/\varepsilon = 0.25$ and $k_{\mathrm{B}}T/\varepsilon = 0.20$ for four number densities $\rho\sigma^3 = 0.01$, 0.05, 0.1 and 0.4. The particles are depicted in red. The Kern–Frenkel interaction bonding volumes are shown as transparent blue regions.

The particle coverage fraction χ is related to the angular semi-amplitude θ by

$$\chi = \sin^2(\theta/2) = \frac{1-\cos(\theta)}{2} \quad (5)$$

The structural and thermodynamic properties and the crystal structures of the aggregates observed in this work are strictly dependent on χ. In the following we specifically analyze three different χ values, one in each section.

III. Patch coverage fraction $\chi = 0.6$

We start our investigation of the phase behavior at $\chi = 0.6$, by performing constant NVT simulations initialized with randomly positioned particles. To visualize the aggregation effects for $\chi = 0.6$, we show in Fig. 3 snapshots of typical configurations for two different temperatures k_BT/ε (with k_B Boltzmann's constant) at increasing number density $\rho\sigma^3$. At $k_BT/\varepsilon = 0.25$, the system consists of small oligomers at both low and high densities. At lower k_BT/ε, the snapshots suggest a different scenario. Fig. 3 shows that the little oligomers transform into large lamellar clusters. The top-right snapshot in Fig. 3 demonstrates the presence of lamellae even at densities as low as $\rho\sigma^3 = 0.01$. No evidence of gas–liquid phase separation is observed for this coverage fraction χ: likely, gas–liquid phase separation is pre-empted by the sudden development of the lamellar phase. We can infer that the relatively high value of the coverage fraction promotes the formation of extended planar structures, lamellae, when the attraction energy becomes sufficiently strong.

To further characterize our system for $\chi = 0.6$, we search for crystal unit cells by using the floppy box method.[50] Within this method, one simulates a small number of particles inside a box that can evolve both in volume and shape. The resulting skewed unit cells form complete crystals upon multiplication in three dimensions but are not necessarily the smallest possible unit cells for the found crystals. To identify the stable structures, we calculate the free energy of the structures that are generated most frequently using the Frenkel–Ladd method,[52] and use thermodynamic integration to explore their stability regions. Additionally, we calculate the fluid free energy using thermodynamic integration. Once a fluid–crystal or crystal–crystal coexistence point is identified, we use Kofke integration to

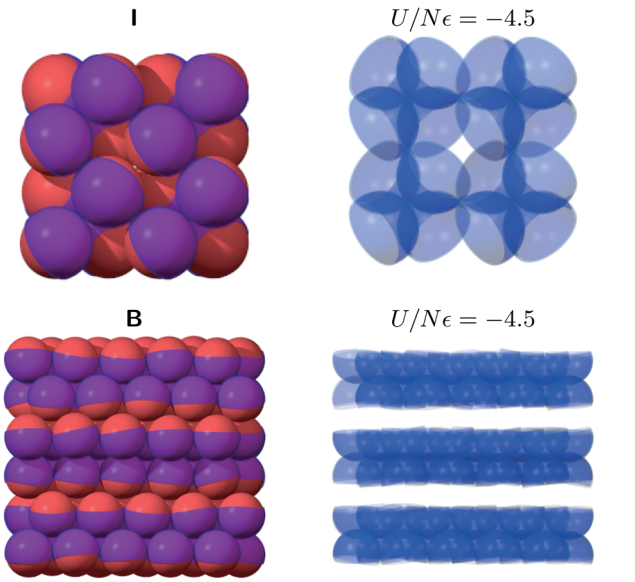

Fig. 5 Stable crystal structures and their ground-state energies for patch coverage fraction $\chi = 0.6$. The particles themselves are depicted in red. The bonding volumes of the particles are shown as transparent blue regions.

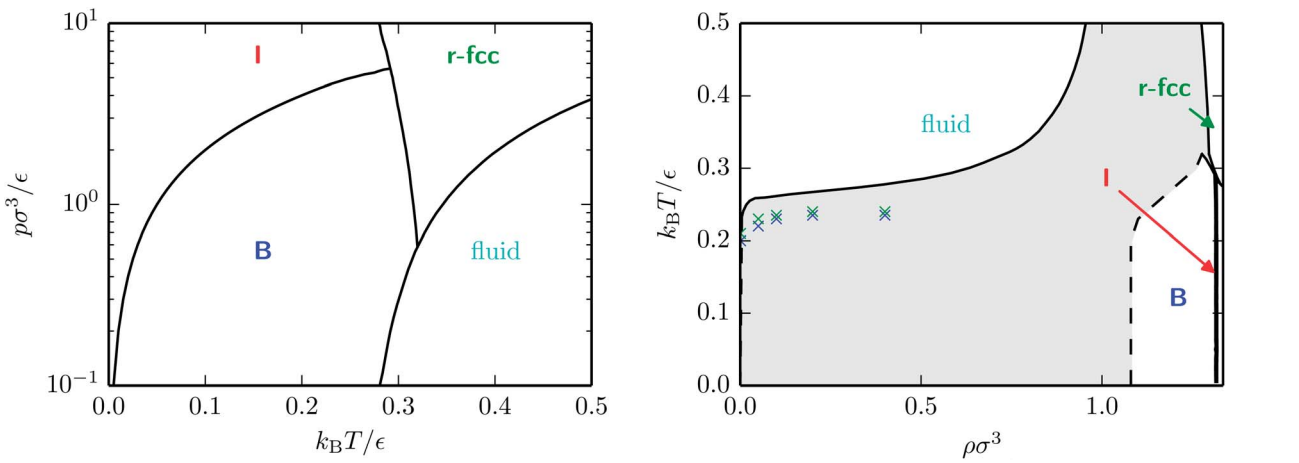

Fig. 4 Equilibrium phase diagrams for $\chi = 0.6$ in T–p and ρ–T representations. In the ρ–T diagram, the gray areas indicate coexistence regions, and the crosses indicate the region where lamellar clusters start forming spontaneously. In particular, for each density the blue crosses denote the highest temperature where, starting from a fluid at a given ρ, we observed lamellar clusters in our NVT simulations. The lowest temperature where we did not observe lamellae is indicated by green crosses. The dashed line is an estimate of where the bilayer sheets start to separate and the crystal breaks up, introducing a finite-size effect, which makes the bilayer sheet coexistence densities difficult to calculate, for further discussion see ref. 49.

follow the coexistence line.[53] A detailed explanation is also given in ref. 49.

The complete equilibrium phase diagrams in the temperature–pressure (T–p) and in the density–temperature (ρ–T) plane are shown in Fig. 4. We identify a stable bilayer crystal structure, which we name **B**, with energy $U/N\varepsilon = -4.5$, corresponding to nine bonded neighbours per particle. The structure is shown in Fig. 5 and it closely resembles the lamellar structures that were found in the constant NVT simulations. The spheres are on a face centered cubic (fcc) lattice and form bilayer sheets that are stacked on top of each other. At high density, yet low temperature, another crystal, labeled as crystal **I** is stable. This structure had already been identified in ref. 49 and it is composed of particles residing on an fcc lattice, with a tetrahedral arrangement of the orientations. At high temperatures we find that the most stable phase is an fcc-crystal with random orientations that we name **r-fcc**, consistent with the hard-sphere behavior expected as $T \to \infty$.

IV. Patch coverage fraction $\chi = 0.5$

We now turn our attention to colloids with a patch coverage fraction of 50%, also known as Janus particles. The phase diagram is shown in Fig. 6 in both the T–p and ρ–T planes.

We observe the same crystal structures as for Janus particles with an interaction range of $\Delta = 0.2\sigma$,[49] although the stability regions are shifted toward higher densities because bonded particles are closer together. Note also that one of the structures coincides with the fcc crystal structure **I** discussed previously for $\chi = 0.6$. The other two structures, (**II** and ***W***), consist of different orientational orderings of particles on a hexagonal close-packed (hcp) lattice and are shown in Fig. 7. We do not find evidence of lamellar structures of the type observed for $\chi = 0.6$. Stable lamellae do not form as particles cannot align side-by-side with all patches interacting sideways. The same holds for slightly smaller coverages, for which we expect a phase behavior close to the Janus case. We also do not observe the wrinkled bilayer sheet phase reported for $\Delta = 0.2\sigma$.[49] Indeed the reduction of the range causes the breaking of the outer bonds which are required to stabilize the wrinkled bilayer sheet phase.

Using SUS simulations, we find a gas–liquid critical point at $k_B T^c/\varepsilon \simeq 0.155$ and $\rho^c\sigma^3 \simeq 0.15$. However, the critical point is

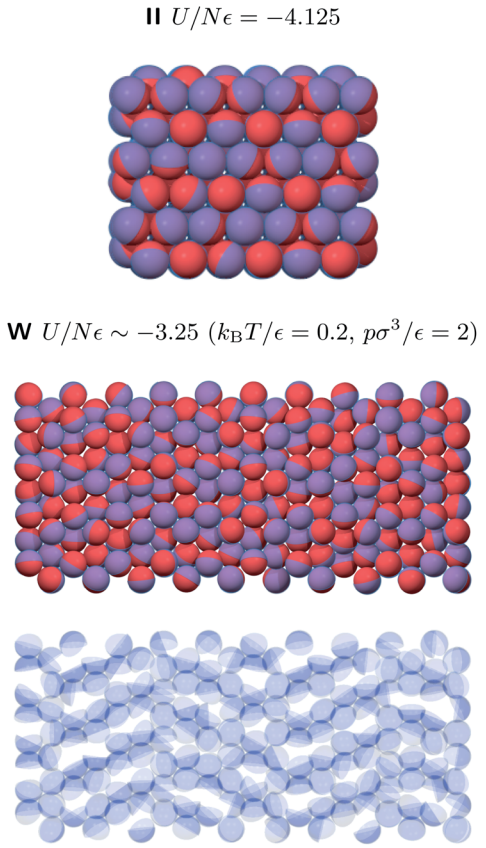

Fig. 7 Typical snapshots of parts of crystals II and W inside a rectangular box for $\chi = 0.5$. The bonding volume is depicted as transparent blue. At the very bottom we show only the bonding volumes of crystal W to indicate its bonding patterns.

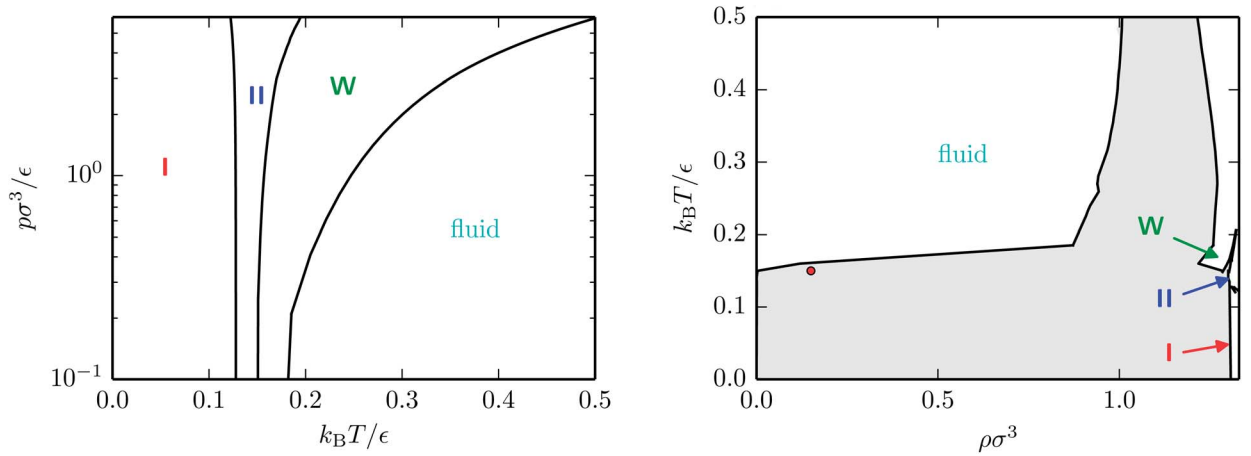

Fig. 6 Equilibrium phase diagram for the Kern–Frenkel model with coverage fraction $\chi = 0.5$ in the T–p and the ρ–T plane. The critical point is marked with a red dot. Note that the critical point is metastable with respect to the fluid–crystal coexistence.

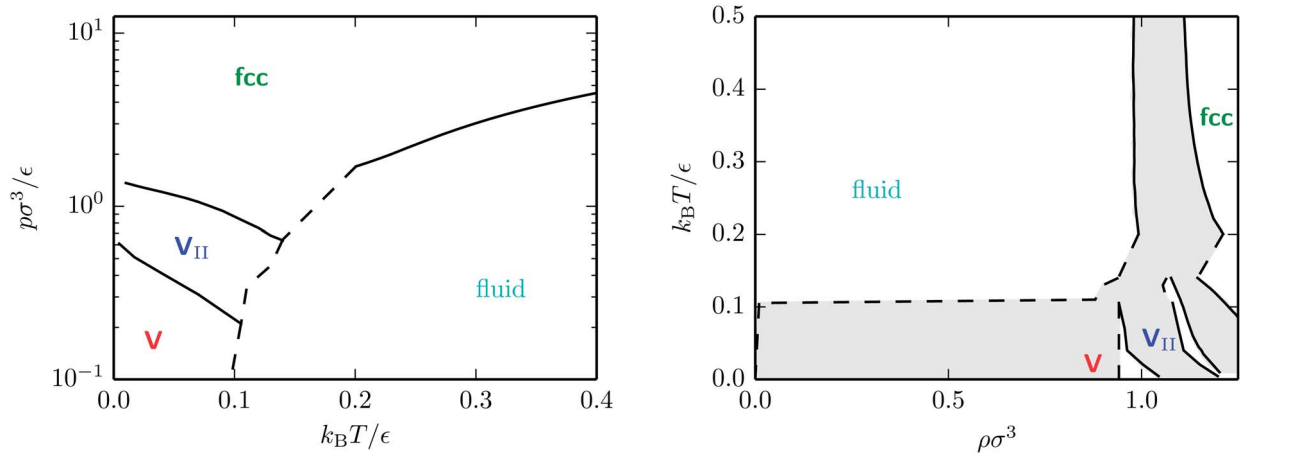

Fig. 8 Phase diagram in the T–p plane and the ρ–T plane for $\chi = 0.3$. The dashed line indicates estimated fluid–crystal coexistence in the region where the fluid could not be equilibrated. The symbols of crystals V and V_{II} are indicated on the left from their stability regions for clarity. The gray areas indicate the coexistence regions.

metastable as it is embedded inside the coexistence region between the low-density fluid and the crystals. We know from previous studies that for $\Delta = 0.5\sigma$ and $\Delta = 0.2\sigma$,[39,49] a critical point has been observed, although in the latter case it was also found to be metastable with respect to the formation of wrinkled bilayer sheets[49].

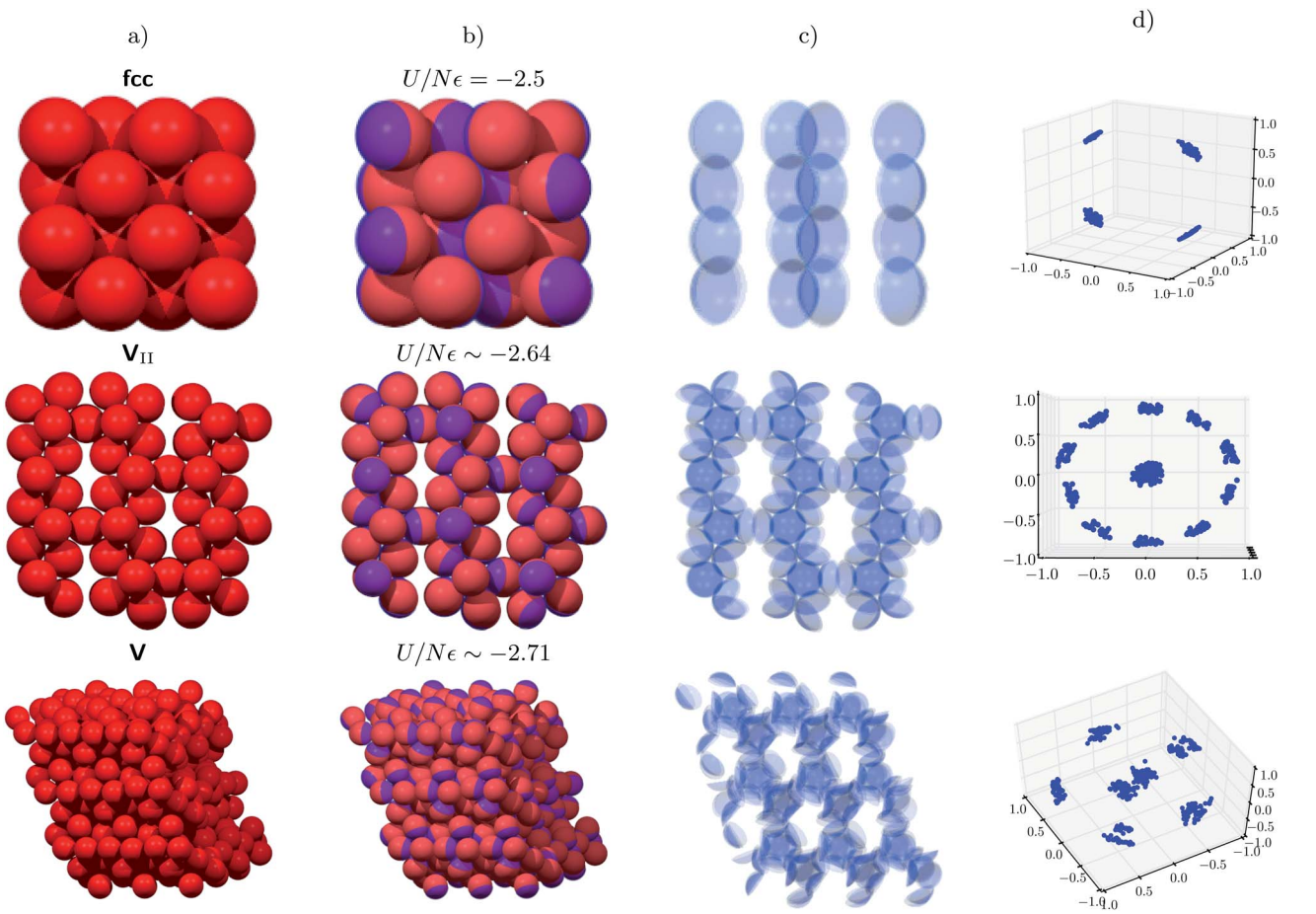

Fig. 9 Stable crystals for coverage fraction $\chi = 0.3$ and their energy per particle in the low-temperature limit. (a) The hard cores of the particles (red); (b) the hard cores of the particles as well as their bonding volumes (transparent blue); (c) only the bonding volumes; (d) the particle orientations depicted on the surface of a unit sphere.

V. Patch coverage fraction $\chi = 0.3$

For a patch coverage fraction of $\chi = 0.3$, we observed a phase behavior, see Fig. 8, that is completely different from that for the higher χ values. We found two 'open' low-energy crystals, and an fcc-based structure, which are all stable in the phase diagram. Of these, we named the open crystal with the lowest energy **V**, since it is composed of a repeating pattern of particles forming a network of connected pentagon-shaped arrangements, each consisting of 7 particles. As shown in Fig. 9a, this structure incorporates large voids. In order to illustrate the pentagonal bonding patterns of the crystal, Fig. 9c shows only the bonding volume of each particle. Interestingly, the network of pentagonal clusters only percolates in two dimensions. The packing in the third dimension is maintained by the pressure. Crystal **V** exists in several polymorphs that all have the same bonding energy, but differ in the way these pentagonal clusters are packed. The second low-energy crystal $\mathbf{V}_{\mathrm{II}}$ is also composed of pentagonal clusters, but the network structure connecting the clusters percolates in three dimensions. The interaction energy of this structure is slightly higher than the one of crystal **V**, making crystal **V** stable in the low temperature limit. As shown in Fig. 9d, both crystals **V** and $\mathbf{V}_{\mathrm{II}}$ have well defined, point-like bond orientations.

The last stable phase identified is an orientationally ordered fcc crystal and we refer to it as **fcc**. This crystal is stable in a large region of the phase diagram, but transforms into a plastic fcc structure at high T.

Of the three stable crystal phases, crystal **V** has the lowest energy ($U/N \approx -2.71\varepsilon$), but the bonds can be satisfied only at relatively low densities. As a result, this structure is stable at low T, but only for low pressure p. Upon increasing p, it is replaced by crystal $\mathbf{V}_{\mathrm{II}}$, which is stable at slightly higher densities, but has a less number of bonds per particle ($U/N \approx -2.64\varepsilon$). Finally, sufficiently high pressures stabilize **fcc**, which has a relatively high energy ($U/N = -2.5\varepsilon$), but can reach a much higher density. The calculated equilibrium phase diagram in the T–p and ρ–T planes is shown in Fig. 8. We note here that it is difficult to calculate the low T fluid–crystal coexistence by means of free energy calculations and thermodynamic integration methods, due to the slow equilibration of the fluid phase. We therefore only approximately estimate the fluid–crystal coexistence locus and indicate it by dashed lines in our phase diagrams. Our approximation is based on the melting temperature of the crystals in NpT simulation and thus provides an upper bound to the thermodynamic line.

In contrast to the case $\Delta = 0.5\sigma$ and a coverage fraction of 30%,[42,54,55] we did not observe tube structures, again pointing to the sensitivity of the phase behavior to the interaction range.

VI. Conclusions

We have presented a simulation study for a one-patch colloidal model with an interaction range of 5% of the particle diameter, focusing on three different values of the patch coverage. In particular, we have identified possible crystal structures and have drawn the resulting equilibrium phase diagrams for patch coverage fractions of 30%, 50% and 60%. This work, together with our previous investigations of the same one-patch model but for larger interaction ranges $\Delta = 0.2\sigma$ (ref. 49) and $\Delta = 0.5\sigma$ (ref. 39 and 42) allows us to gauge how the range and the angular width of the patch affect the phase behavior.

For a coverage fraction $\chi = 0.6$, free-energy calculations of the crystal structures generated by the floppy box method have identified three different stable crystal phases: a bilayer sheet structure and two fcc structures, one orientationally ordered and one orientationally disordered. The bilayer structure is stable at intermediate densities and low temperatures and coexists with the fluid phase in a wide range of densities. Inside the coexistence region, the stable situation would be a phase separation between a bilayer crystal and a low density fluid. However, in experiments, one might expect floating bilayer sheets to form spontaneously in the fluid. In fact, within this range of densities the coexistence region between the bilayers and the fluid is rather large and extends down to very low densities. Within this range of densities, constant NVT simulations have shown the formation of small oligomers that suddenly rearrange themselves in bilayer clusters upon cooling, showing that the nucleation of bilayer structures from the fluid does not require large activation energy.

The Janus case, corresponding to $\chi = 0.5$, shows a rather different phase behavior: the lamellar phases are not formed because patches are not wide enough for particles to attract each other in a side-by-side configuration. Of the crystals, only the ordered fcc phase, stable at low T, is identical to the one observed for $\chi = 0.6$. The range does not seem to strongly affect the observed crystal structures. Indeed we observe the same stable crystals as for Janus particles with a longer interaction range $\Delta = 0.2\sigma$.[49] However, we do not recover the wrinkled bilayer phase reported in ref. 49 since the interaction range is now too short to stabilize the structure. With successive umbrella sampling, we have located a gas–liquid critical point which is found to be metastable with respect to the fluid–crystal coexistence, as for the $\Delta = 0.2\sigma$ case.

Finally, we have investigated particles with a significantly smaller patch coverage fraction, namely $\chi = 0.3$. For this case, we found that the two most stable crystal structures at low temperature are actually 'open' crystals made up out of connected pentagon-shaped clusters. Upon increasing temperature or pressure, these crystals cease to exist, in favor of the fcc structure. We note that for $\chi = 0.3$ but with a longer interaction range $\Delta = 0.5\sigma$, particles self-assemble into rigid tubular structures[42] which are not seen here. Evidently, our interaction range is too short to stabilize these structures.

The comparison between the results reported in this article and the one previously published[49] offers an exhaustive description of the role played by the bond geometry in one-patch particles. The width and the range of the patch determine the maximum number of bonds each particle can form, and particularly the low temperature bonding patterns. This results in an extremely strong sensitivity of the phase diagram of this class of particles to relatively small changes in the patch size. As shown here, small changes in χ drastically change the self-assembly at low-densities as well as the stability of the

high-density crystal structures. We also note that some of the thermodynamically stable structures require a large number of particles in the unit cell, making it impossible to use assumptions to predict the relevant crystal phases. As shown in the present work, numerical simulations can aid in the discovery of such structures. The sensitivity of the bond geometry is not limited to the patch coverage but is equally relevant to the selection of the patch range. A clear example is provided by the disappearance of the wrinkled sheet phase from the phase diagram on going from $\Delta = 0.2\sigma$ to $\Delta = 0.05\sigma$. Given the fact that fine-tuning these parameters experimentally is still a challenge, the knowledge of the effects of the patch range and coverage on the phase behavior will be crucial in interpreting future experimental observations of these particles. Finally, we note that the effects on the phase behaviour of polydispersity in patch-size, hard-core size and interaction length could be an interesting subject of further investigations.

Acknowledgements

Parts of the work are also presented in the PhD thesis of Z. Preisler. The authors gratefully acknowledge ERC-226207-PATCHYCOLLOIDS (T. Vissers, G. Munaò, F. Smallenburg and F. Sciortino), ITN-234810-COMPLOIDS (Z. Preisler) and MIUR-PRIN (F. Sciortino).

References

1 V. N. Manoharan, M. T. Elsesser and D. J. Pine, *Science*, 2003, **301**, 483–487.
2 S. C. Glotzer and M. J. Solomon, *Nat. Mater.*, 2007, **6**, 557–562.
3 Z. Zhang and S. C. Glotzer, *Nano Lett.*, 2004, **4**, 1407–1413.
4 A. P. R. Eberle, R. Castañeda-Priego, J. M. Kim and N. J. Wagner, *Langmuir*, 2012, **28**, 1866.
5 Q. Meng, Y. Kou, X. Ma, Y. Liang, L. Guo, C. Ni and K. Liu, *Langmuir*, 2012, **28**, 5017.
6 T. H. Zhang, J. Klok, R. H. Tromp, J. Groenewold and W. K. Kegel, *Soft Matter*, 2012, **8**, 667.
7 S. Sacanna and D. J. Pine, *Curr. Opin. Colloid Interface Sci.*, 2011, **16**, 96.
8 Q. Chen, J. Yan, J. Zhang, S. C. Bae and S. Granick, *Langmuir*, 2012, **28**, 1355.
9 Y. Jing, B. Moses, B. Sung Chul, L. Erik and G. Steve, *Nature*, 2012, **491**, 578–581.
10 A. Walther and A. H. E. Muller, *Chem. Rev.*, 2013, **113**, 5194–5261.
11 I. C. Pons-Siepermann and S. C. Glotzer, *Soft Matter*, 2012, **8**, 6226.
12 A. B. Pawar and I. Kretzschmar, *Macromol. Rapid Commun.*, 2010, **31**, 150–168.
13 E. Bianchi, R. Blaak and C. Likos, *Phys. Chem. Chem. Phys.*, 2011, **13**, 6297.
14 A. Giacometti, *Cent. Eur. J. Phys.*, 2012, **10**, 540–551.
15 E. Bianchi, J. Largo, P. Tartaglia, E. Zaccarelli and F. Sciortino, *Phys. Rev. Lett.*, 2006, **97**, 168301–168304.
16 F. Sciortino and E. Zaccarelli, *Curr. Opin. Colloid Interface Sci.*, 2011, **15**, 246.
17 C. Gögelein, F. Romano, F. Sciortino and A. Giacometti, *J. Chem. Phys.*, 2012, **136**, 094512.
18 F. Smallenburg and F. Sciortino, *Nat. Phys.*, 2013, **9**, 554–558.
19 J. M. Tavares, P. I. C. Teixeira and M. M. Telo da Gama, *Phys. Rev. E: Stat., Nonlinear, Soft Matter Phys.*, 2009, **80**, 021506.
20 J. M. Tavares, P. I. C. Teixeira, M. M. T. da Gama and F. Sciortino, *J. Chem. Phys.*, 2010, **132**, 234502.
21 J. M. Tavares, P. I. C. Teixeira and M. M. Telo da Gama, *Mol. Phys.*, 2009, **107**, 453–466.
22 F. Romano, E. Sanz and F. Sciortino, *J. Chem. Phys.*, 2010, **132**, 184501.
23 F. Romano, E. Sanz and F. Sciortino, *J. Chem. Phys.*, 2011, **134**, 174502.
24 Z. Zhang, A. S. Keys, T. Chen and S. C. Glotzer, *Langmuir*, 2005, **21**, 11547.
25 A.-P. Hynninen, J. H. Thijssen, E. C. Vermolen, M. Dijkstra and A. Van Blaaderen, *Nat. Mater.*, 2007, **6**, 202–205.
26 F. Romano and F. Sciortino, *Nat. Commun.*, 2012, **3**, 975.
27 K.-H. Roh, D. C. Martin and J. Lahann, *Nat. Mater.*, 2005, **4**, 759–763.
28 B. Wang, B. Li, B. Zhao and C. Y. Li, *J. Am. Chem. Soc.*, 2008, **130**, 11594–11595.
29 C.-H. Chen, R. K. Shah, A. R. Abate and D. A. Weitz, *Langmuir*, 2009, **25**, 4320–4323.
30 A. M. Jackson, J. W. Myerson and F. Stellacci, *Nat. Mater.*, 2004, **3**, 330–336.
31 W. L. Miller and A. Cacciuto, *Phys. Rev. E: Stat., Nonlinear, Soft Matter Phys.*, 2009, **80**, 021404.
32 Q. Chen, J. K. Whitmer, S. Jiang, S. C. Bae, E. Luijten and S. Granick, *Science*, 2011, **331**, 199.
33 S. Jiang, Q. Chen, M. Tripathy, E. Luijten, K. S. Schweizer and S. Granick, *Adv. Mater.*, 2010, **22**, 1060–1071.
34 A. Walther and A. H. E. Muller, *Soft Matter*, 2008, **4**, 663–668.
35 B. Ren, A. Ruditskiy, J. H. Song and I. Kretzschmar, *Langmuir*, 2011, **28**, 1149–1156.
36 S. Gangwal, A. Pawar, I. Kretzschmar and O. D. Velev, *Soft Matter*, 2010, **6**, 1413–1418.
37 B. J. Park, T. Brugarolas and D. Lee, *Soft Matter*, 2011, **7**, 6413–6417.
38 N. Glaser, D. J. Adams, A. Böker and G. Krausch, *Langmuir*, 2006, **22**, 5227–5229.
39 F. Sciortino, A. Giacometti and G. Pastore, *Phys. Rev. Lett.*, 2009, **103**, 237801.
40 G. Rosenthal, K. E. Gubbins and S. H. Klapp, *J. Chem. Phys.*, 2012, **136**, 174901.
41 G. Munaó, D. Costa, F. Sciortino and C. Caccamo, *J. Chem. Phys.*, 2011, **134**, 194502.
42 Z. Preisler, T. Vissers, F. Smallenburg, G. Munaò and F. Sciortino, *J. Phys. Chem. B*, 2013, **117**, 9540–9547.
43 N. Kern and D. Frenkel, *J. Chem. Phys.*, 2003, **118**, 9882–9889.
44 A. Giacometti, F. Lado, J. Largo, G. Pastore and F. Sciortino, *J. Chem. Phys.*, 2009, **131**, 174114.
45 A. Giacometti, F. Lado, J. Largo, G. Pastore and F. Sciortino, *J. Chem. Phys.*, 2010, **132**, 174110.

46 F. Sciortino, A. Giacometti and G. Pastore, *Phys. Chem. Chem. Phys.*, 2010, **12**, 11869–11877.
47 Q. Chen, S. C. Bae and S. Granick, *Nature*, 2011, **469**, 381–384.
48 Y. Iwashita and Y. Kimura, *Soft Matter*, 2013, **9**, 10694–10698.
49 T. Vissers, Z. Preisler, F. Smallenburg, M. Dijkstra and F. Sciortino, *J. Chem. Phys.*, 2013, **138**, 164505.
50 L. Filion, M. Marechal, B. van Oorschot, D. Pelt, F. Smallenburg and M. Dijkstra, *Phys. Rev. Lett.*, 2009, **103**, 188302.
51 P. Virnau and M. Müller, *J. Chem. Phys.*, 2004, **120**, 10925–10930.
52 D. Frenkel and A. J. C. Ladd, *J. Chem. Phys.*, 1984, **81**, 3188–3193.
53 D. A. Kofke, *J. Chem. Phys.*, 1993, **98**, 4149–4162.
54 G. Munaò, Z. Preisler, T. Vissers, F. Smallenburg and F. Sciortino, *Soft Matter*, 2013, **9**, 2652–2661.
55 T. Vissers, F. Smallenburg, G. Munaò, Z. Preisler and F. Sciortino, *J. Chem. Phys.*, 2014, **140**, 144902.